Conformational Equilibria of Alkanes in Aqueous Solution: Relationship to Water Structure Near Hydrophobic Solutes

Henry S. Ashbaugh,* Shekhar Garde,# Gerhard Hummer,# Eric W. Kaler,* and Michael E. Paulaitis§

*Department of Chemical Engineering and Center for Molecular and Engineering Thermodynamics, University of Delaware, Newark, Delaware 19716, #Theoretical Biology and Biophysics T-10, MS K710, Los Alamos National Laboratory, Los Alamos, New Mexico 87545, and §Department of Chemical Engineering, The Johns Hopkins University, Baltimore, Maryland 21218

ABSTRACT   Conformational free energies of butane, pentane, and hexane in water are calculated from molecular simulations with explicit waters and from a simple molecular theory in which the local hydration structure is estimated based on a proximity approximation. This proximity approximation uses only the two nearest carbon atoms on the alkane to predict the local water density at a given point in space. Conformational free energies of hydration are subsequently calculated using a free energy perturbation method. Quantitative agreement is found between the free energies obtained from simulations and theory. Moreover, free energy calculations using this proximity approximation are approximately four orders of magnitude faster than those based on explicit water simulations. Our results demonstrate the accuracy and utility of the proximity approximation for predicting water structure as the basis for a quantitative description of n-alkane conformational equilibria in water. In addition, the proximity approximation provides a molecular foundation for extending predictions of water structure and hydration thermodynamic properties of simple hydrophobic solutes to larger clusters or assemblies of hydrophobic solutes.

INTRODUCTION

Dating back to the iceberg hypothesis of Frank and Evans (1945), molecular explanations of hydrophobic phenomena have been sought, based on the unique tetrahedral hydrogen-bonding structure of water. Manifestations of hydrophobic phenomena include the limited solubility and aggregation of nonpolar solutes in water (Blokzijl and Engberts, 1993; Tanford, 1980), as well as self-assembly processes, such as protein folding (Dill, 1990; Kauzmann, 1959) and micelle formation (Hunter, 1987; Israelachvili, 1992), that are thought to be driven in large part by hydrophobic interactions. Indeed, many of the successful molecular theories describing hydrophobic effects for simple nonpolar solutes have incorporated into their framework either the structure of bulk liquid water or the microscopic structure of waters of hydration in the vicinity of such solutes (Hummer et al., 1996b; Lazaridis and Paulaitis, 1992; Pohorille and Pratt, 1990; Pratt and Chandler, 1977; Pratt and Pohorille, 1992; Stillinger, 1973).

In the Pratt–Chandler theory, for example, the experimental water oxygen–oxygen radial distribution function is used within an Ornstein–Zernike-like formalism to calculate both solute–water and solute–solute correlations for nonpolar solutes in water (Pratt and Chandler, 1977). The solute–water correlations are subsequently used in a perturbative approach to calculate the thermodynamics of hydrophobic hydration. More recently, an information theory model of hydration has been used to calculate the free energy of forming a cavity the size and shape of the solute in water— the dominant contribution to the solute chemical potential—by modeling water density fluctuations within molecular-sized volumes in liquid water (Hummer et al., 1996b). Applications of the information theory model provide a quantitative understanding of the dependence of hydrophobic effects on temperature and pressure that have led to insights into heat (Garde et al., 1999; Garde et al., 1996a) and pressure (Hummer et al., 1998) denaturation of proteins. This approach, however, has limited applicability for molecularly large and mesoscopic solutes, because the probability of spontaneously forming a large cavity in liquid water becomes vanishingly small, and, more fundamentally, Gaussian-like descriptions of molecular scale fluctuations become inaccurate. Subtle effects, such as the cavity expulsion potential (Hummer and Garde, 1998), and, at larger length scales, dewetting phenomena (Stillinger, 1973; Wallqvist and Berne, 1995; Lum and Luzar, 1997; Lum and Chandler, 1998; Lum et al., 1999) must be considered for a complete description of the hydration of molecularly large hydrophobic solutes.

Lazaridis and Paulaitis, on the other hand, demonstrated that the large negative entropy and large positive heat capacity increments characteristic of hydrophobic hydration of simple solutes at ambient temperature can be calculated from solute–water translational and orientational pair correlations alone (Lazaridis and Paulaitis, 1992, 1993, 1994; Paulaitis et al., 1994). Their approach provides a direct connection between the molecular structure and the macroscopic thermodynamics of hydration. However, the accurate calculation of solute–water translational and orientational

correlations becomes increasingly difficult for solutes of increasing size and structural complexity, and prohibitive for solutes with internal conformational degrees of freedom.

Recent simulations of a variety of hydrated nonpolar solutes with different geometries show that water structure in the vicinity of these solutes is only locally sensitive to the structural details of the solute (Ashbaugh and Paulaitis, 1996; Garde et al., 1996b). Hence, a hierarchy of n-site proximity approximations has been proposed to describe water structure near a molecular (i.e., multisite) solute in terms of water correlations with only the nearest n sites of the solute (Garde et al., 1996b). These proximity approximations represent an extension of the proximity criterion introduced by Ben-Naim (1974) in the context of generalized molecular distribution functions, and implemented by Beveridge and coworkers (Mehrotra and Beveridge, 1980; Mezei and Beveridge, 1986) to characterize water structure around hydrated molecular solutes. Pettitt and coworkers (Pettitt et al., 1998; Makarov et al., 1998) review the implementation of proximal radial distribution functions to protein hydration.

The proximity approximations, in some sense, have parallels to linear surface area correlations for the free energy of hydration (Chothia, 1974; Hermann, 1972; Reynolds et al., 1974; Sitkoff et al., 1994), although these correlations do not describe the solute–water interface in sufficient detail to provide a unique relationship between free energy and molecular topology (Ashbaugh et al., 1998; Ashbaugh et al., in preparation). Water structure, however, can be highly sensitive to local solute structure (Cheng and Rossky, 1998), and it is precisely these details of molecular structure that are accounted for in the proximity approximations.

We have shown in previous work that the proximity approximations provide an accurate description of water structure in the vicinity of molecular hydrophobic solutes, and further, that this water structure can be used to accurately predict the large negative entropies of hydrophobic hydration (Ashbaugh and Paulaitis, 1996; Garde et al., 1996b), as well as hydrophobic driving forces for the aggregation of nonpolar solutes in water (Garde et al., 1996c). In this paper, we explore the accuracy of water structures predicted by the two-site proximity approximation for calculating conformational free energies of n-alkanes in water. Our approach is to compare conformational free energies of hydration calculated from the free energy perturbation method of Zwanzig (1954) using explicit water simulations to those calculated using the proximity approximation. The accuracy and enhanced computational speed of the proximity approximation relative to the explicit water simulations demonstrate the utility of this simple molecular theory of hydration from which thermodynamic properties of hydrophobic interactions can be derived.

THEORY AND METHODS

Molecular simulations

We calculate the hydration contribution to the conformation-dependent free energy of three linear alkanes in water:

butane, pentane, and hexane. Exploration of the entire dihedral angle space of pentane and hexane using explicit water simulations is computationally too expensive. Hence, we calculate only the change in hydration free energy corresponding to well-defined reaction paths for these two n-alkanes.

Canonical ensemble Monte Carlo (MC) simulations (Allen and Tildesley, 1987) were carried out for aqueous solutions consisting of a single n-alkane molecule in a bath of 216 water molecules at 25°C and a density of 0.997 g/cm^3. Lennard–Jones (LJ) interactions for the alkane CH$_3$ and CH$_2$ groups were modeled using the optimized potentials for liquid simulations (OPLS) united-atom parameters (Table 1) (Jorgensen et al., 1984). Alkane internal bond lengths and bond angles were constrained to 1.53 Å and 109.5°, respectively. Water was modeled using the simple point charge (SPC) potential (Table 1) (Berendsen et al., 1981). The LJ parameters for solute–water interactions were obtained from geometric mean combining rules. Electrostatic interactions were evaluated using the generalized reaction-field method introduced by Hummer et al. (1994). Both LJ and generalized reaction-field minimum image interactions were truncated on a site-by-site basis at one-half the simulation box length. Conformational reaction paths were considered that connect the extended all-*trans* conformations to the alternating *gauche* conformations of pentane ($tt \rightarrow gg'$) and hexane ($ttt \rightarrow gg'g$). [Note: The letters t and g denote the ideal *trans* ($\varphi = 180°$) and *gauche* ($\varphi = \pm 60°$) backbone dihedral conformations, respectively. g' differentiates between the two mirror image *gauche* conformers, g^+ and g^-, along the same alkane chain. For example, the designation tg denotes the set of equivalent pentane conformers $\{tg^+, tg^-, g^+t, g^-t\}$, whereas gg' denotes the conformers $\{g^+g^-, g^-g^+\}$.] These reaction paths are given in Table 2, and the initial and final conformational states of pentane and hexane are depicted in Fig. 1. Two independent reaction paths corresponding to the $ttt \rightarrow gg'g$ transition for hexane were considered to evaluate the path independence of the calculated free energy changes. The compact gg' and $gg'g$ conformations of pentane and hexane, respectively, are inaccessible in reality due to unfavorable intrachain overlap, i.e., the pentane effect (Mattice and Suter, 1994). We note, however, that solvent contributions

TABLE 1 Optimized potentials for liquid simulations (Jorgensen, et al., 1984) and simple point charge (Berendsen, et al., 1981) interaction parameters for the alkane united-atom groups and water oxygens

Interacting Pair	σ (Å)	ϵ (kcal/mol)
CH$_2$—CH$_2$	3.905	0.118
CH$_3$—CH$_3$	3.905	0.175
CH$_4$—CH$_4$	3.73	0.294
O—O	3.16557	0.1554

σ and ϵ are the Lennard–Jones diameter and well depth, respectively. Geometric mean combining rules were used to calculate cross solute–water interaction parameters, i.e., $\sigma_{ij} = (\sigma_{ii}\sigma_{jj})^{1/2}$ and $\epsilon_{ij} = (\epsilon_{ii}\epsilon_{jj})^{1/2}$.

TABLE 2   *n*-Alkane conformational reaction paths

	φ_1	φ_2	φ_3
Butane			
1) $t \rightarrow g$	variable	—	—
Pentane			
2) a $tt \rightarrow gt$	variable	180°	—
b $gt \rightarrow gg'$	60°	variable	—
Hexane			
3) a $ttt \rightarrow tg't$	180°	variable	180°
b $tg't \rightarrow gg't$	variable	−60°	180°
c $gg't \rightarrow gg'g$	60°	−60°	variable
4) a $ttt \rightarrow gtt$	variable	180°	180°
b $gtt \rightarrow gtg$	60°	180°	variable
c $gtg \rightarrow gg'g$	60°	variable	60°

The dihedral angles are numbered consecutively down the *n*-alkane backbone.

to the free energy, which are our interest here, are, by definition, independent of the intrachain energy.

During the simulations, each solute was held in a fixed conformation along a given reaction path, and the relative hydration free energy difference between this reference conformation and a perturbed solute conformation, $\Delta A_{\text{hyd}}(\varphi \rightarrow \varphi + \delta\varphi)$, was evaluated using the free energy perturbation expression (Zwanzig, 1954),

$$\Delta A_{\text{hyd}}(\varphi \rightarrow \varphi + \delta\varphi)$$
$$= -kT \ln\langle\exp[-\beta\Delta E(\varphi \rightarrow \varphi + \delta\varphi)]\rangle_\varphi, \quad (1)$$

where $\beta^{-1} = kT$ is the product of Boltzmann's constant and the absolute temperature, and ΔE is the solute–water potential energy difference between the perturbed, $\varphi + \delta\varphi$, and the reference, φ, conformations. The angle brackets, $\langle\cdots\rangle_\varphi$,
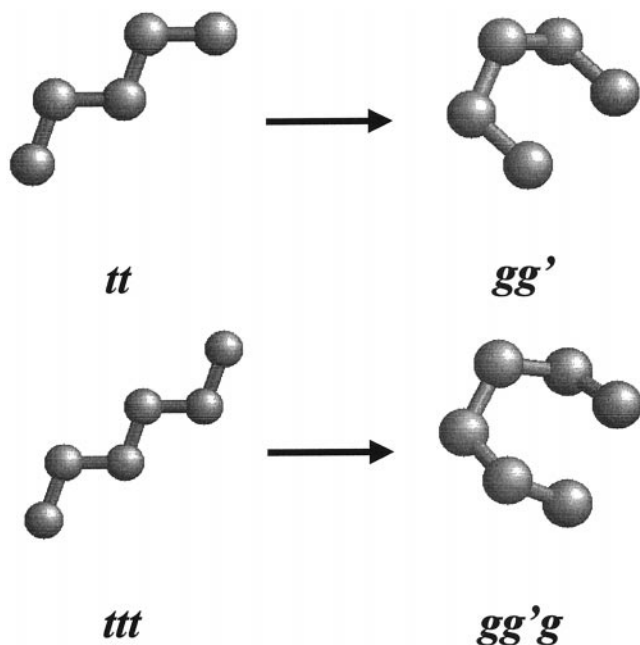

FIGURE 1   Schematic illustration of the all *trans* (*tt* and *ttt*) and alternating *gauche* (*gg'* and *gg'g*) conformations for pentane and hexane.

denote thermal averaging over solvent configurations generated for the solute in the reference conformation. A simulation for one conformation of butane in water consisted of 40,000 MC passes for equilibration followed by 80,000 MC passes for sampling (1 MC pass = 216 attempted water and 4 attempted solute moves). A simulation for one conformation of pentane or hexane in water consisted of 40,000 MC passes for equilibration followed by 200,000 MC passes for sampling. Twenty-four solute conformations from $\varphi = -172.5°$ to $+172.5°$ in 15° increments were simulated along each reaction path with $\delta\varphi = \pm7.5°$.

Path independence of the free energy guarantees that $\Delta A_{\text{hyd}}(-180° \rightarrow 180°) = 0$. However, this does not necessarily hold for free energies calculated from simulation because only a finite portion of the total configurational space is sampled. Therefore, we report $\Delta A_{\text{hyd}}(-180° \rightarrow 180°)$ as a simple measure of the uncertainty in the simulation calculations. This hysteresis error was subtracted from the reported hydration free energies assuming a linear dependence of the error on φ. The rotation of a single dihedral angle through 360° along each of the reaction paths in Table 2 required approximately 7 CPU days on a DEC AlphaStation 255/300.

Free energy calculations using the proximity approximation

The perturbation expression, Eq. 1, can be expanded in terms of cumulants of the distribution of ΔE in the reference state (Hummer et al., 1995b, 1996c; Kubo, 1962; Smith and van Gunsteren, 1994; Zwanzig, 1954). For sufficiently small perturbations in φ, i.e., for $\Delta E \ll kT$, the first order term provides an accurate approximation to the corresponding change in free energy,

$$\Delta A_{\text{hyd}}(\varphi \rightarrow \varphi + \delta\varphi) \approx \langle\Delta E(\varphi \rightarrow \varphi + \delta\varphi)\rangle_\varphi, \quad (2)$$

which is exact in the limit, $\delta\varphi \rightarrow 0$ (Chandler, 1987). The ensemble average for $\langle\Delta E\rangle_\varphi$ in this equation is related to the water structure surrounding the solute in its reference conformation by

$$\langle\Delta E\rangle_\varphi = \int \Delta E \times \rho(\mathbf{r}_{\text{W}}|\{\mathbf{r}_1, \ldots, \mathbf{r}_n\}_\varphi) \, d\mathbf{r}_{\text{W}}, \quad (3)$$

where $\rho(\mathbf{r}_{\text{W}}|\{\mathbf{r}_1, \ldots, \mathbf{r}_n\}_\varphi)$ is the number density of water molecules at $\mathbf{r}_{\text{W}}$ given that the sites of an *n*-site solute in conformation φ are situated at $\{\mathbf{r}_1, \ldots, \mathbf{r}_n\}_\varphi$. For an *n*-site solute,

$$\Delta E(\varphi \rightarrow \varphi + \delta\varphi) = \sum_{i=1}^{n}[\Phi(\mathbf{r}_{\text{W}}, \mathbf{r}_{i,\varphi+\delta\varphi}) - \Phi(\mathbf{r}_{\text{W}}, \mathbf{r}_{i,\varphi})],$$
$$(4)$$

where $\Phi(\mathbf{r}_{\text{W}}, \mathbf{r}_{i,\varphi})$ is the interaction energy between a water molecule at $\mathbf{r}_{\text{W}}$ and the *i*th solute site at $\mathbf{r}_{i,\varphi}$ in conformation φ. In the following, we provide details of the proximity

approximation and solute–water interactions used to calculate $\rho(\mathbf{r}_W|\{\mathbf{r}_1, \cdots, \mathbf{r}_n\}_\varphi)$ and ΔE, respectively, in the integrand of Eq. 3.

Proximity approximation

The inhomogeneous density of water in the vicinity of a solute is obtained from the solute–water potential-of-mean force (PMF), which, for a multisite solute, can be expressed as an expansion in terms of one-particle, two-particle, and higher-order multiparticle PMFs between the solute sites and a water molecule (Green, 1952; Hummer and Soumpasis, 1994a, 1994b). This expansion, truncated at the level of two- or three-particle correlations, has been applied successfully to strongly associating inhomogeneous systems, such as ion density distributions near nucleic acids (Klement et al., 1991; Soumpasis, 1984), the ice–water interface (Hummer and Soumpasis, 1994a), and biomolecular hydration (García et al., 1997; Garde et al., 1997; Hummer et al., 1995a, 1996a; Hummer and Soumpasis, 1994b). However, for the hydration of hydrophobic solutes, where volume exclusion is the dominant solute–water interaction, it was found that the PMF expansion, truncated at the level of three-particle correlations, substantially overestimates water densities at contact (Garde et al., 1996b). Unreasonably large water densities (more than 50 times the bulk density) were likewise noted near the alanine dipeptide using the PMF expansion truncated at the level of two-particle correlations (Pelligrini and Doniach, 1995; Pelligrini et al., 1996). On the other hand, the proximity approximations correctly account for the excluded volume of overlapping solute sites, thereby providing an accurate representation of the solute–water PMF for weakly interacting, hydrophobic solutes (Garde et al., 1996b)

In the one-site proximity approximation, the solute–water PMF is given by the PMF between water and only the nearest site of the solute, assuming solute sites of equal size. Thus,

$$\rho(\mathbf{r}_W|\{\mathbf{r}_1, \ldots, \mathbf{r}_n\}_\varphi) \approx \rho_b g(\mathbf{r}_W, \mathbf{r}_j), \qquad (5)$$

where j is the solute site closest to a water molecule at $\mathbf{r}_W$, ρ_b is the bulk water density, and $g(\mathbf{r}_W, \mathbf{r}_j)$ is the pair correlation function between water and a lone solute site. Similarly, for the two-site proximity approximation,

$$\rho(\mathbf{r}_W|\{\mathbf{r}_1, \ldots, \mathbf{r}_n\}_\varphi) \approx \rho_b g(\mathbf{r}_W|\mathbf{r}_j, \mathbf{r}_k), \qquad (6)$$

where k is the second nearest solute site to a water molecule at $\mathbf{r}_W$, and $g(\mathbf{r}_W|\mathbf{r}_j, \mathbf{r}_k)$ is the conditional triplet correlation function between a water molecule and a lone pair of solute sites located at $\mathbf{r}_j$ and $\mathbf{r}_k$. These approximations are readily generalizable to n sites. It is straightforward to confirm that, for a solute composed of n sites, the n-site proximity approximation is exact. We use the two-site proximity approximation for water density predictions throughout this work and refer to it hereafter simply as the proximity approximation.

Triplet correlations between a water oxygen and two solute sites, $g(\mathbf{r}_W|\mathbf{r}_j, \mathbf{r}_k)$, were evaluated from a series of MC simulations of two OPLS united-atom methanes in SPC water with the methanes held at separations varied in increments of 0.2 Å from 1.2 to 6.6 Å. Triplet correlations at intermediate separations were approximated using tri-linear interpolation. Details of these simulations are given elsewhere (Garde et al., 1996b).

Interaction potentials

In the explicit water simulations, OPLS united-atom potentials were used for the CH_2 and CH_3 interactions with SPC water. Water structures predicted using the proximity approximation, however, assume that all the alkane sites are OPLS united-atom methanes. Because liquid structure is determined primarily by repulsive interactions and the OPLS repulsive core of all the alkane sites are similar, differences in water structure between the various solute sites are not expected to be significant. However, small differences in the free energy calculated using the proximity approximation are expected if methane–water interactions are used in the energy calculations. To account for differences between the OPLS LJ well depths, we used modified solute–water interactions in Eq. 4 following a strategy similar to that in Weeks–Chandler–Andersen perturbation theory (Weeks et al., 1971):

$$\Phi_{CH_iO}(r)$$

$$= \begin{cases} 4\epsilon\left[\left(\dfrac{\sigma}{r}\right)^{12} - \left(\dfrac{\sigma}{r}\right)^6\right] + \epsilon - \epsilon_{CH_iO} & r < 2^{1/6}\sigma \\[2ex] 4\epsilon_{CH_iO}\left[\left(\dfrac{\sigma}{r}\right)^{12} - \left(\dfrac{\sigma}{r}\right)^6\right] & r > 2^{1/6}\sigma, \end{cases} \qquad (7)$$

where $\epsilon = \epsilon_{CH_4O}$, $r = r_{CH_4O}$, and $i = 2$ or 3 specifies the CH_2 and CH_3 sites of an n-alkane, respectively. Thus, the repulsive core of CH_i-water interactions are assumed to be the same as that for CH_4-water interactions, whereas the attractive CH_4-water interactions have been normalized to the potential minimum for CH_i-water interactions.

The free energy changes for $\delta\varphi$ perturbations along a particular reaction path were calculated by integrating Eq. 3 using the solute–water potentials in Eq. 7 with water densities predicted from the proximity approximation in Eq. 6. This integration was performed using a grid placed within a rectangular box that extended 10 Å from the minimum and maximum x, y, and z coordinates of the solute in its extended conformation. The calculated free energy values are sensitive to the integration parameters, the grid spacing, and the value of $\delta\varphi$ along a reaction path. We found that, for a grid spacing of ~0.25 Å and $\delta\varphi = \pm 3.75°$, the calculated free energies are independent of the integration parameters. This grid spacing is close to the bin width of 0.20 Å used for calculating triplet correlations. Increasing the dimensions of the box did not change our results because the long-range contributions to the LJ interaction potential are small and

essentially independent of conformation, and thereby cancel when calculating ΔE in Eq. 3. Approximately one CPU minute was required to calculate the free energy profile along each reaction path on an SGI R10K processor. This corresponds to an increase in computational speed over the explicit water simulations of approximately four orders of magnitude.

RESULTS AND DISCUSSION

Calculated free energies of hydration are shown in Figs. 2 through 5 as a function of n-alkane conformation for the reaction paths in Table 2. For butane (Fig. 2), the free energy of hydration increases with increasing backbone dihedral angle from the compact *cis* ($\varphi_1 = 0°$) to the extended *trans* ($\varphi_1 = 180°$) conformation. This characteristic behavior has been reported in a large body of simulation (Ashbaugh et al., 1998; Beglov and Roux, 1994; Jorgensen, 1982; Jorgensen and Buckner, 1987; Kaminski et al., 1994; Rosenberg et al., 1982; Tobias and Brooks, 1990) and theoretical (Hummer et al., 1996b; Pratt and Chandler, 1977; Zichi and Rossky, 1986) studies of butane conformations in water, and is consistent with the notion embodied in linear free energy–surface area correlations that hydrophobic interactions tend to minimize the extent of solvent-accessible surface area of hydrophobic solutes. Differences in the methods and interaction potentials used here and in previous studies, however, preclude quantitative comparisons with previous work.
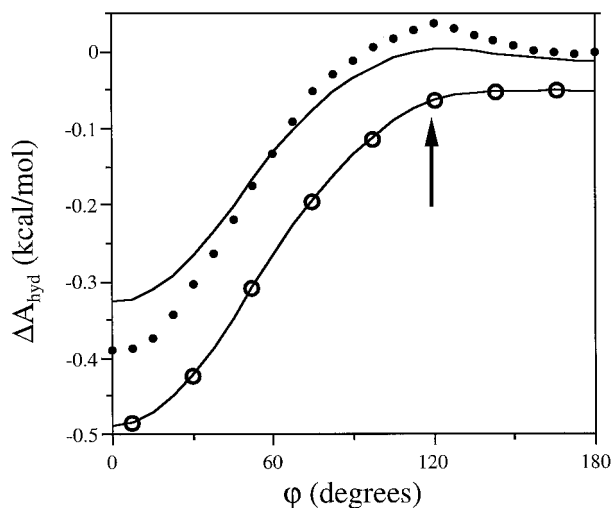
For pentane (Fig. 3), $\Delta A_{\mathrm{hyd}}(\varphi_1, 180°)$ is symmetric about $\varphi_1 = 0°$ with each half of the free energy profile essentially the same as that obtained for butane. Moreover, the depth of the free energy minimum at $\varphi_1 = 0°$ is approximately the same as that obtained for the *cis* conformation of butane, as might be expected, because holding φ_2 fixed at $180°$ minimizes the interaction between the terminal methyl groups of pentane along this reaction path. In contrast, holding φ_1 fixed at $60°$ while rotating φ_2 results in a partial overlap of the terminal methyl groups along the $gt \rightarrow gg'$ reaction path. Consequently, $\Delta A_{\mathrm{hyd}}(60°, \varphi_2)$ is asymmetric about $\varphi_2 = 0°$, and the free energy minimum at $\varphi_2 \approx -30°$ is more than twice that for $\Delta A_{\mathrm{hyd}}(\varphi_1, 180°)$. In this case, the terminal methyl groups make their closest approach in the gg' conformation (Fig. 1), which roughly corresponds to this free energy minimum.

For hexane along reaction path 3 (Fig. 4), φ_3 is held fixed at $180°$ in steps 3a and 3b, which effectively reduces the influence of the terminal methyl group adjacent to this dihedral angle. As a consequence, the free energy profiles $\Delta A_{\mathrm{hyd}}(180°, \varphi_2, 180°)$ and $\Delta A_{\mathrm{hyd}}(\varphi_1, -60°, 180°)$ are virtually indistinguishable from $\Delta A_{\mathrm{hyd}}(\varphi_1, 180°)$ and $\Delta A_{\mathrm{hyd}}(60°, \varphi_2)$ for pentane, respectively, with the exception that $\Delta A_{\mathrm{hyd}}(\varphi_1, -60°, 180°)$ and $\Delta A_{\mathrm{hyd}}(60°, \varphi_2)$ are mirror images of one another because of solute symmetry. When φ_3 is rotated in step 3c of this reaction path, a minimum in the free energy profile is observed at $\varphi_3 = 30°$ that is much lower than the minima observed for butane or pentane. We attribute this deep minimum to the partial overlap of the terminal methyl groups, as well as the hydration contribution to the attraction between the methyl group adjacent to

FIGURE 2 The conformation-dependent hydration free energy of butane following reaction path 1 (Table 2). ●, simulation result; *line*, prediction using the proximity approximation including attractive interactions (Eq. 7); ○, the proximity approximation predictions excluding attractive interactions (Eq. 8). The simulation results are referenced to $\Delta A_{\mathrm{hyd}}(180°) = 0$. The proximity approximation predictions excluding attractive interactions have been shifted downward for clarity. The arrow denotes the location of the free energy maximum in both the simulation results and proximity approximation predictions. The simulation hysteresis error is smaller than the symbols.
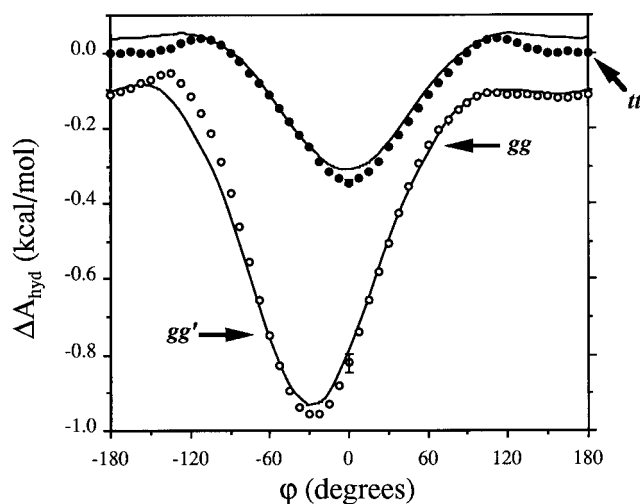

FIGURE 3 The conformation-dependent hydration free energy of pentane following reaction paths 2a and b (Table 2). ● and ○, simulation results for reaction paths 2a and b, respectively; The lines are the two-site proximity approximation predictions. The locations of the *tt*, *gg*, and *gg'* conformations are identified on this figure for clarity. The simulation results are referenced to $\Delta A_{\mathrm{hyd}}(180°, 180°) = 0$. The cumulative simulation hysteresis errors, $\Delta A_{\mathrm{hyd}}(-180° \rightarrow 180°)$, are indicated by the error bars at $\varphi = 0°$.
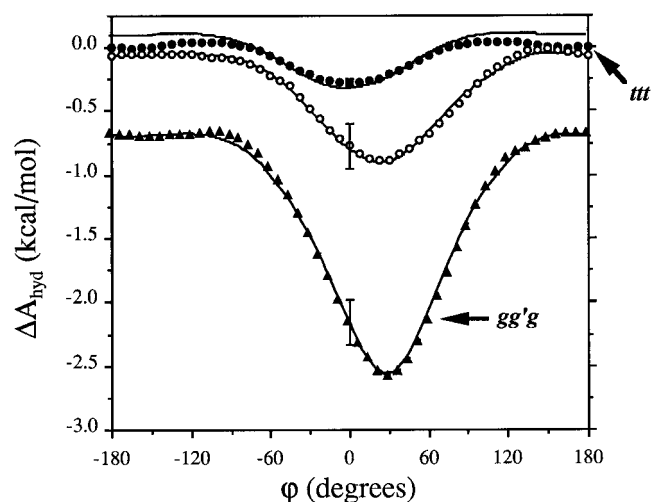
FIGURE 4 The conformation-dependent hydration free energy of hexane following reaction paths 3a–c (Table 2). Shown are the simulation results for reaction paths 3a (●), 3b (○), and 3c (▲). The lines are the two-site proximity approximation predictions. The locations of the *ttt* and *gg′g* conformations are identified on this figure for clarity. The simulation results are referenced to $\Delta A_{\text{hyd}}(180°, 180°, 180°) = 0$. The cumulative simulation hysteresis errors, $\Delta A_{\text{hyd}}(-180° \rightarrow 180°)$, are indicated by the error bars at $\varphi = 0°$.

φ_3 and the methylene group attached to the methyl group at the other end of the chain.

For hexane along reaction path 4 (Fig. 5), φ_2 is held fixed at 180° in steps 4a and 4b, which has the effect of isolating conformations at each end of the alkane chain. Hence, changes in the hydration free energy for rotations of φ_1 and φ_3 are virtually independent of one another and $\Delta A_{\text{hyd}}(\varphi_1,$
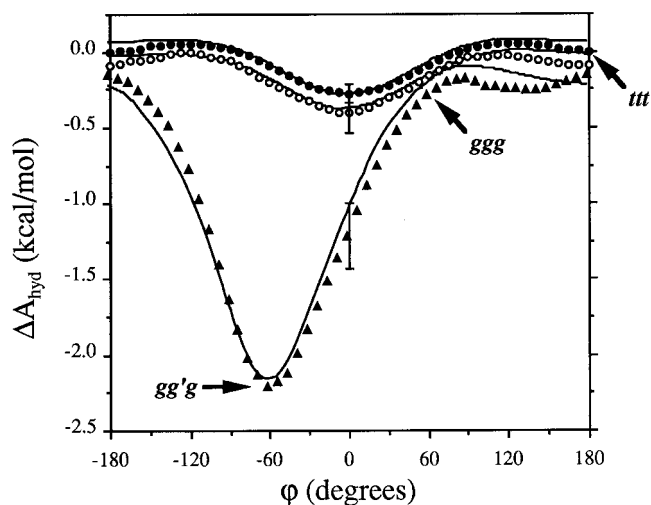

FIGURE 5 The conformation-dependent hydration free energy of hexane following reaction paths 4a–c (Table 2). Shown are the simulation results for reaction paths 4a (●), 4b (○), and 4c (▲). The lines are the two-site proximity approximation predictions. The locations of the *ttt*, *ggg*, and *gg′g* conformations are identified on this figure for clarity. The simulation results are referenced to $\Delta A_{\text{hyd}}(180°, 180°, 180°) = 0$. The cumulative simulation hysteresis errors, $\Delta A_{\text{hyd}}(-180° \rightarrow 180°)$, are indicated by the error bars at $\varphi = 0°$.

$180°, 180°)$ and $\Delta A_{\text{hyd}}(60°, 180°, \varphi_3)$ are qualitatively similar to the free energy profile of butane. The largest free energy change occurs in step 4c due to the overlap of the opposing CH_3CH_2 groups, which gives a favorable hydration free energy contribution. In this case, the deep minimum at $\varphi_2 = -60°$ accounts for most of the change in free energy along the entire reaction path.

All free energy calculations using the water structure predicted from the proximity approximation are in excellent agreement with the profiles obtained from simulation. Systematically larger discrepancies are noted for butane and the butane-like reaction paths of pentane and hexane (reaction paths 1, 2a, 3a, 4a, and 4b). However, the absolute differences between the simulation and proximity results for the butane-like reaction paths are, in general, small compared to the overall change in free energy for pentane and hexane.

A general characteristic of all the free energy profiles is the presence of weak maxima observed near the rim of the free energy wells (e.g., see simulation results in Fig. 2 near $\varphi_1 \approx 120°$). This feature is observed for both the explicit water simulation results and the proximity approximation predictions, although it is not as prominent for the proximity approximation. To gain insight into the origin of this characteristic behavior, we calculated the conformational free energy of hydration for butane using the proximity approximation and the purely repulsive Weeks–Chandler–Andersen interaction potential for methane (Weeks et al., 1971),

$$\Phi_{\text{CH}_i\text{O}}(r)$$

$$= \begin{cases} 4\epsilon_{\text{CH}_4\text{O}}\left[\left(\dfrac{\sigma_{\text{CH}_4\text{O}}}{r}\right)^{12} - \left(\dfrac{\sigma_{\text{CH}_4\text{O}}}{r}\right)^{6}\right] + \epsilon_{\text{CH}_4\text{O}} & r < 2^{1/6}\sigma_{\text{CH}_4\text{O}} \\ 0 & r > 2^{1/6}\sigma_{\text{CH}_4\text{O}}. \end{cases}$$

(8)

The results are plotted in Fig. 2. For the purely repulsive interaction potential, the predicted free energy minimum for the *cis* conformation is deeper than that obtained when attractive interactions are included. More importantly, the maximum at $\varphi_1 \approx 120°$ disappears. Similar observations were made for the hydration free energy profiles of pentane and hexane (not shown). We conclude, therefore, that the weak maxima result mainly from the opposing effects of solute–water attractive and repulsive interactions. The attractive interactions favor extended alkane conformations, whereas the repulsive hydrophobic interactions favor compact alkane conformations. The free energy maxima correspond to conformations for which these solute–water interactions offset one another.

We noted above that hysteresis errors arise in explicit simulations due to insufficient sampling of phase space in simulations of finite length. Similar hysteresis errors can arise in the free energies calculated using the proximity approximation. One reason for this error is that the triplet correlation functions themselves are evaluated from explicit water simulations of finite length, and as such, contain statistical uncertainties. A second source of hysteresis error

arises because the triplet correlation functions are available only at discrete water–methane and methane–methane separations. Finally, hysteresis errors can arise even if the triplet correlation functions are known exactly, and result from the inherent approximations of using only lower order correlation functions to calculate the inhomogeneous density of water surrounding the solute. These errors, when combined with the numerical integration of Eq. 3 and discrete perturbations, $\delta\varphi$, lead to a systematic error at each step along a reaction path.

Nonetheless, we find that, for most of the reaction paths considered here, the net change in free energy for rotating a single dihedral angle through 360° is zero. The one exception is step 4c in which a CH_3CH_2 group of hexane is moved as a rigid body. In this case, we observe a net decrease of 0.6 kcal/mol in the free energy for $\varphi_2 = -180° \rightarrow 180°$. Moreover, this hysteresis error can be reproduced by rotating a CH_3CH_2 group along this reaction path in the absence of the rest of the hexane molecule. Thus, we conclude that the hysteresis error in our free energy predictions is amplified along reaction paths for which multiple sites of the solute are moved as a rigid body. This error can be reduced by choosing reaction paths such that only a limited number of solute sites are perturbed in each step. We also suggest making quantitative evaluations of the hysteresis error for reaction paths involving multisite perturbations, as was done here. For the free energy calculations reported here for step 4c, we have subtracted the corresponding estimate of the hysteresis error to obtain the free energy profiles in Fig. 5, which are in excellent agreement with the explicit water simulation results.

The calculated change in hydration free energy for the conformational rearrangement of each alkane chain from the extended all-*trans* conformation (*t*, *tt*, and *ttt*) to the alternating *gauche* (*gg′* and *gg′g*) or the helical *gauche* (*g*, *gg*, and *ggg*) conformation is reported in Table 3. Overall, the free energies calculated using the proximity approximation are in excellent agreement with those obtained from simulation. With the exception of butane and the pentane *tt* → *gg* transition, this agreement is within the simulation uncertainties; for butane the free energy change is within twice the uncertainty, and for the pentane *tt* → *gg* transition, the difference is only 0.07 kcal/mol or approximately 0.1 *kT*. Moreover, we find that the free energy changes for the hexane *ttt* → *gg′g* transition calculated for the two independent reaction paths are in close agreement with each other and their differences are within the simulation uncertainties, thus verifying the path independence of the hydration free energy. We note that the proximity approximation also gives slightly different free energies for this transition along the two hexane reaction paths. Nonetheless, the agreement is excellent.

A point-by-point comparison of hydration free energies calculated from explicit water simulations and from the proximity approximation is shown in Fig. 6 for the two hexane reaction paths. All points fall close to the diagonal line with a root mean square difference of 0.1 *kT* between

TABLE 3 Calculated changes in the free energy of hydration for *trans–gauche* conformational transitions of the *n*-alkanes

Alkane and Reaction Path		Explicit Water Simulations	Proximity Approximation
Butane			
$t \rightarrow g$		−0.133 (0.005)	−0.122
Pentane			
$tt \rightarrow gg'$		−0.75 (0.02)	−0.77
$tt \rightarrow gg$		−0.24 (0.02)	−0.31
Hexane			
$ttt \rightarrow gg'g$	reaction path 3	−2.14 (0.19)	−2.21
	reaction path 4	−2.21 (0.22)	−2.24
$ttt \rightarrow ggg$	reaction path 4	−0.29 (0.22)	−0.28

Free energies are reported in units of kcal/mol. The numbers in parentheses are simulation hysteresis errors.

the free energies over the entire range of hexane conformations. This root mean square difference is more than three times smaller than the statistical uncertainties reported in Table 3 for the explicit water simulations along either reaction path. Thus, the two methods are in excellent agreement.

In Fig. 7, the conformational free energy of hydration of hexane, obtained from simulation, is plotted as a function of its van der Waals surface area. The van der Waals surface was chosen rather than the solvent-accessible surface or the molecular surface (Lee and Richards, 1971; Richards, 1977) because it was found to give the most accurate linear free energy–surface area correlation for *n*-alkane conformations in water (Ashbaugh et al., 1998). The strong correlation between free energy and van der Waals surface area depicted in Fig. 7 is clearly not a linear correlation. Indeed, we
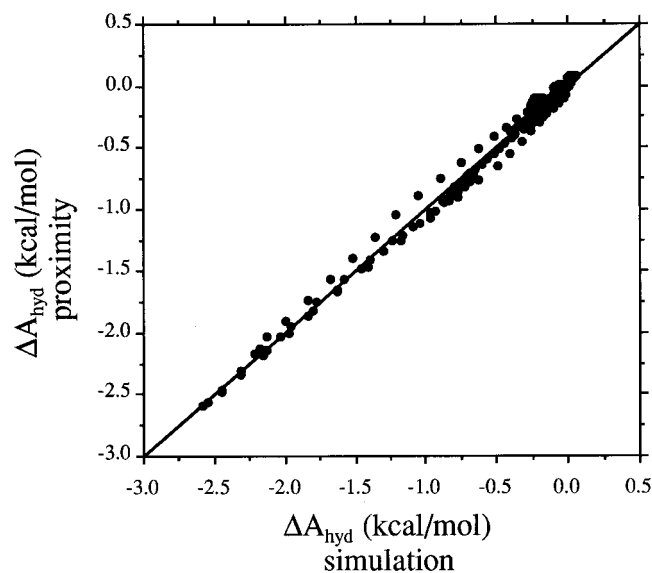

FIGURE 6 Comparison of the hydration free energies of hexane reaction paths 3a–c and 4a–c determined from simulation and the proximity approximation. The root mean square difference between the free energies calculated using these techniques is 0.06 kcal/mol.
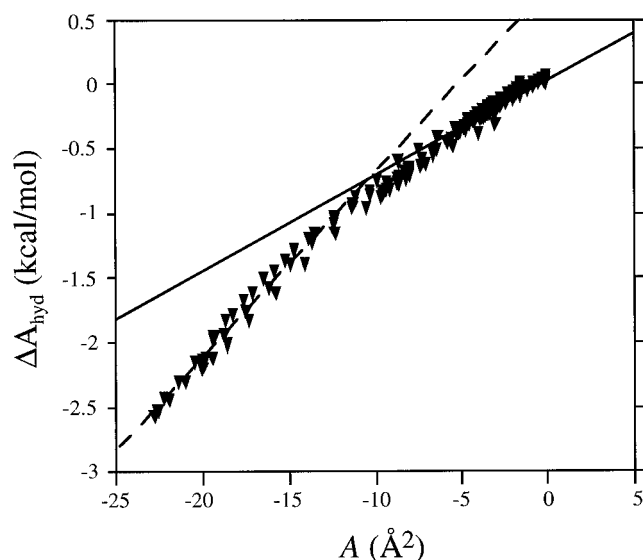
FIGURE 7   Conformational free energy of hydration of hexane (reaction paths 3a–c and 4a–c) obtained from simulation as a function of the van der Waals surface area of hexane. The surface area and ΔA_{hyd} are referenced to zero in the all *trans* conformation.

find that the free energy–surface area coefficient, γ, in the linear relation,

$$\Delta A_{hyd} = \gamma A + b, \tag{9}$$

differs by a factor of two for the all-*trans* conformation and the $gg'g$ conformation of hexane. Thus, to achieve accuracies in the conformational free energy of hydration comparable to those obtained from the proximity approximation, typical linear free energy–surface area correlations would require a conformationally dependent γ which, in fact, cannot be extracted from measured transfer free energies for the *n*-alkanes. Moreover, we expect the conformational dependence of γ found in Fig. 7 to be specific to hexane, and therefore, not transferable to a wider range of hydrocarbons.

CONCLUSIONS

Most simulation studies of hydrophobic effects to date have focused mainly on water-mediated interactions between simple nonpolar solutes, such as the PMF between methane pairs (Lüdemann et al., 1997, 1996; New and Berne, 1995; Pangali et al., 1979; Payne et al., 1997; Smith and Haymet, 1993; van Belle and Wodak, 1993; Young and Brooks, 1997) or the conformational equilibrium of a single butane chain in water (Ashbaugh et al., 1998; Beglov and Roux, 1994; Jorgensen, 1982; Jorgensen and Buckner, 1987; Kaminski et al., 1994; Rosenberg et al., 1982; Tobias and Brooks, 1990). Although these studies add substantially to our understanding of the hydrophobic driving forces for small nonpolar solutes in aqueous solution, few unifying concepts have resulted which permit the extension of molecular hydrophobic effects to larger clusters or assemblies of nonpolar solutes.

The proximity approximation presented herein may provide such a connection. We have shown that the two-site proximity approximation leads to quantitative predictions of the conformational equilibria of *n*-alkanes in water, in contrast to conventional free energy–surface area correlations, which are at best approximate in nature, or the truncated PMF expansion, which, in previous work, was shown to substantially overestimate water densities around nonpolar solutes. We conclude, therefore, that the underlying assumption of the proximity approximation is correct, at least for relatively simple molecular solutes, such as the *n*-alkanes considered here; that is, the inhomogeneous structure of water is only locally sensitive to the molecular details of a hydrophobic solute. Although we expect this assumption to break down for macroscopic interfaces where water structure is strongly perturbed, the length scale at which this occurs has not yet been determined. Indeed, our preliminary results for much larger clusters of 135 methanes in water indicate that the proximity approximation gives a quantitatively accurate description of water structure around these assemblies as well (Ashbaugh and Paulaitis, unpublished results).

Although the one-site proximity approximation has been shown, in previous work, to account largely for the water structure in the vicinity of a single nonpolar solute in water (Ashbaugh and Paulaitis, 1996; Garde et al., 1996b), the basic unit for accurate determination of water-mediated forces is the methane dimer in aqueous solution (Garde et al., 1996c). Indeed, the two-site proximity approximation used in conjunction with free energy perturbation yields the exact PMF between a methane pair in water, whereas the one-site approximation does not (Garde et al., 1996c). Although the triplet correlation functions required for the two-site proximity approximation represent an initial computational cost that is significant, these correlation functions are determined only once. Subsequent applications of the proximity approximation can be accomplished much faster by referencing this existing library of triplet correlation functions. For the *n*-alkane solutes studied here, we observed an enhancement in computational speed of nearly four orders of magnitude.

REFERENCES

Allen, M. P., and D. J. Tildesley. 1987. Computer Simulation of Liquids. Oxford University Press, Oxford, U.K.

Ashbaugh, H. S., E. W. Kaler, and M. E. Paulaitis. 1998. Hydration and conformational equilibria of simple hydrophobic and amphiphilic solutes. *Biophys. J.* 75:755–768.

Ashbaugh, H. S., and M. E. Paulaitis. 1996. Entropy of hydrophobic hydration: extension to hydrophobic chains. *J. Phys. Chem.* 100: 1900–1913.

Beglov, D., and B. Roux. 1994. Finite representation of an infinite bulk system: solvent boundary potential for computer simulations. *J. Chem. Phys.* 100:9050–9063.

Ben-Naim, A. 1974. Water and Aqueous Solutions. Plenum Press, New York.

Berendsen, H. J. C., J. P. M. Postma, W. F. van Gunsteren, and J. Hermans. 1981. Interaction models of water in relation to protein hydration. *In* Intermolecular Forces: Proceedings of the Fourteenth Jerusalem Symposium on Quantum Chemistry and Biochemistry. B. Pullman, editor. D. Reidel Publishing Company, Dordrecht, The Netherlands. 331–342.

Blokzijl, W., and J. B. F. N. Engberts. 1993. Hydrophobic effects. Opinions and facts. *Agnew. Chem. Int. Ed. Engl.* 32:1545–1579.

Chandler, D. 1987. Introduction to Modern Statistical Mechanics. Oxford University Press, New York.

Cheng, Y.-K., and P. J. Rossky. 1998. Surface topography dependence of biomolecular hydrophobic hydration. *Nature.* 392:696–699.

Chothia, C. 1974. Hydrophobic bonding and accessible surface area in proteins. *Nature.* 248:338–339.

Dill, K. A. 1990. Dominant forces in protein folding. *Biochemistry.* 29: 7133–7155.

Frank, H. S., and M. W. Evans. 1945. Free volume and entropy in condensed systems. III. Entropy in binary liquid mixtures; partial molal entropy in dilute solutions; structure and thermodynamics in aqueous electrolytes. *J. Chem. Phys.* 13:507–532.

García, A. E., G. Hummer, and D. M. Soumpasis. 1997. Hydration of an alpha-helical peptide: comparison of theory and molecular dynamics simulation. *Proteins Strut. Funct. Genet.* 27:471–480.

Garde, S., G. Hummer, A. E. García, M. E. Paulaitis, and L. R. Pratt. 1996a. Origin of the entropy convergence in hydrophobic hydration and protein folding. *Phys. Rev. Lett.* 77:4966–4968.

Garde, S., G. Hummer, A. E. García, L. R. Pratt, and M. E. Paulaitis. 1996b. Hydrophobic hydration: inhomogeneous water structure near nonpolar molecular solutes. *Phys. Rev. E.* 53:R4310–R4313.

Garde, S., G. Hummer, and M. E. Paulaitis. 1996c. Hydrophobic interactions: conformational equilibria and the association of non-polar molecules in water. *Faraday Disc.* 103:125–139.

Garde, S., G. Hummer, M. E. Paulaitis, and A. E. García. 1997. Hydration of biological macromolecules: from small solutes to proteins and nucleic acids. *In* Proceedings of the 1996 Materials Research Society Fall Meeting Symposium on Statistical Mechanics in Physics and Biology. D. Wirtz, T. C. Halsey, editors. Materials Research Society, Pittsburgh. 463:21–28.

Garde, S., A. E. García, L. R. Pratt, and G. Hummer. 1999. Temperature dependence of the solubility of nonpolar gases in water. *Biophys. Chem.* 78:21–32.

Green, H. S. 1952. The Molecular Theory of Fluids. North-Holland Publishing Company, Amsterdam, The Netherlands.

Hermann, R. B. 1972. Theory of hydrophobic bonding. II. The correlation of hydrocarbon solubility with solvent cavity surface area. *J. Phys. Chem.* 76:2754–2759.

Hummer, G., A. E. García, and D. M. Soumpasis. 1995a. Hydration of nucleic-acid fragments: comparison of theory and experiment for high-resolution crystal structures of RNA, DNA, and DNA-drug complexes. *Biophys. J.* 68:1639–1652.

Hummer, G., A. E. García, and D. M. Soumpasis. 1996a. A statistical mechanical description of biomolecular hydration. *Faraday Disc.* 103: 175–189.

Hummer, G., and S. Garde. 1998. Cavity expulsion and weak dewetting of hydrophobic solutes in water. *Phys. Rev. Lett.* 80:4193–4196.

Hummer, G., S. Garde, A. E. García, M. E. Paulaitis, and L. R. Pratt. 1998. The pressure dependence of hydrophobic interactions is consistent with the observed pressure denaturation of proteins. *Proc. Natl. Acad. Sci. USA.* 95:1552–1555.

Hummer, G., S. Garde, A. E. García, A. Pohorille, and L. R. Pratt. 1996b. An information theory model of hydrophobic interactions. *Proc. Natl. Acad. Sci. USA.* 93:8951–8955.

Hummer, G., L. R. Pratt, and A. E. García. 1995b. The hydration free energy of water. *J. Phys. Chem.* 99:14188–14194.

Hummer, G., L. R. Pratt, and A. E. García. 1996c. The free energy of ionic hydration. *J. Phys. Chem.* 100:1206–1215.

Hummer, G., and D. M. Soumpasis. 1994a. Computation of the water density distribution at the ice–water interface using the potentials-of-mean-force expansion. *Phys. Rev. E.* 49:591–596.

Hummer, G., and D. M. Soumpasis. 1994b. A statistical mechanical treatment of the structural hydration of biological macromolecules: results for B-DNA. *Phys. Rev. E.* 50:5085–5095.

Hummer, G., D. M. Soumpasis, and M. Neumann. 1994. Computer simulation of aqueous Na-Cl electrolytes. *J. Phys.: Condens. Matt.* 6:A141–A144.

Hunter, R. J. 1987. Foundations of Colloid Science. Oxford University Press, Oxford, U.K.

Israelachvili, J. 1992. Intermolecular and Surface Forces. Academic Press Limited, London.

Jorgensen, W. L. 1982. Monte Carlo simulation of *n*-butane in water: conformational evidence for the hydrophobic effect. *J. Chem. Phys.* 77:5757–5765.

Jorgensen, W. L., and J. K. Buckner. 1987. Use of statistical perturbation theory for computing solvent effects on molecular conformation. Butane in water. *J. Phys. Chem.* 91:6083–6085.

Jorgensen, W. L., J. D. Madura, and C. J. Swenson. 1984. Optimized intermolecular potential functions for liquid hydrocarbons. *J. Am. Chem. Soc.* 106:6638–6646.

Kaminski, G., E. M. Duffy, T. Matusui, and W. L. Jorgensen. 1994. Free energies of hydration and pure liquid properties of hydrocarbons from the OPLS all-atom model. *J. Phys. Chem.* 98:13077–13082.

Kauzmann, W. 1959. Some factors in the interpretation of protein denaturation. *Adv. Protein Chem.* 14:1–63.

Klement, R., D. M. Soumpasis, and T. M. Jovin. 1991. Computation of ionic distributions around charged biomolecular structures: results for right-handed and left-handed DNA. *Proc. Natl. Acad. Sci. USA.* 88: 4631–4635.

Kubo, R. 1962. Generalized cumulant expansion method. *J. Phys. Soc. Jpn.* 17:1100–1120.

Lazaridis, T., and M. E. Paulaitis. 1992. Entropy of hydrophobic hydration: a new statistical mechanical formulation. *J. Phys. Chem.* 96:3847–3855.

Lazaridis, T., and M. E. Paulaitis. 1993. Reply to the comment on "Entropy of hydrophobic hydration: a new statistical mechanical formulation". *J. Phys. Chem.* 97:5789–5790.

Lazaridis, T., and M. E. Paulaitis. 1994. Simulation studies of the hydration entropy of simple, hydrophobic solutes. *J. Phys. Chem.* 98:635–642.

Lee, B., and F. M. Richards. 1971. Protein structures: estimation of static accessibility. *J. Mol. Bio.* 55:379–400.

Lüdemann, S., R. Abseher, H. Schreiber, and O. Steinhauser. 1997. The temperature dependence of hydrophobic association in water. Pair versus bulk hydrophobic interactions. *J. Am. Chem. Soc.* 119:4206–4213.

Lüdemann, S., H. Schreiber, R. Abseher, and O. Steinhauser. 1996. The influence of temperature on pairwise hydrophobic interactions of methane-like particles: a molecular dynamics study of the free energy. *J. Chem. Phys.* 104:286–295.

Lum, K., and A. Luzar. 1997. Pathway to surface-induced phase-transition of a confined fluid. *Phys. Rev. E* 56:R6283–R6286.

Lum, K., and D. Chandler. 1998. Phase-diagram and free energies of vapor films and tubes for a confined fluid. *Int. J. Thermophysics.* 19:845–855.

Lum, K., D. Chandler, and J. D. Weeks. 1999. Hydrophobicity at small and large length scales. *J. Phys. Chem.* in press.

Makarov, V. A., B. K. Andrews, and B. M. Pettitt. 1998. Reconstructing the protein–water interface. *Biopolymers.* 45:469–478.

Mattice, W. L., and U. W. Suter. 1994. Conformational Theory of Large Molecules: The Rotational Isomeric State Model in Macromolecular Systems. John Wiley and Sons, Inc., New York.

Mehrotra, P. K., and D. L. Beveridge. 1980. Structural analysis of molecular solutions based on quasi-component distribution functions. Application to [H_2CO]$_{aq}$ at 25°C. *J. Am. Chem. Soc.* 102:4287–4294.

Mezei, M., and D. L. Beveridge. 1986. Structural chemistry of biomolecular hydration via computer simulation: the proximity criterion. *Methods Enzymol.* 127:21–47.

New, M. H., and B. J. Berne. 1995. Molecular dynamics calculation of the effect of solvent polarizability on the hydrophobic interaction. *J. Am. Chem. Soc.* 117:7172–7179.

Pangali, C., M. Rao, and B. J. Berne. 1979. A Monte Carlo simulation of the hydrophobic interaction. *J. Chem. Phys.* 71:2975–2981.

Paulaitis, M. E., H. S. Ashbaugh, and S. Garde. 1994. The entropy of hydration of simple hydrophobic solutes. *Biophys. Chem.* 51:349–357.

Payne, V. A., N. Matubayasi, L. R. Murphy, and R. M. Levy. 1997. Monte Carlo study of the effect of pressure on hydrophobic association. *J. Phys. Chem. B.* 101:2054–2060.

Pelligrini, M., and S. Doniach. 1995. Modeling solvation contributions to conformational free energy changes of biomolecules using a potential of mean force expansion. *J. Chem. Phys.* 103:2696–2702.

Pelligrini, M., N. Grønbech-Jensen, and S. Doniach. 1996. Potentials of mean force for biomolecular simulations: theory and test on alanine dipeptide. *J. Chem. Phys.* 104:8639–8648.

Pettitt, M. B., V. A. Makarov, and B. K. Andrews. 1998. Protein hydration density: theory, simulations and crystallography. *Curr. Opin. Struct. Biol.* 8:218–221.

Pohorille, A., and L. R. Pratt. 1990. Cavities in molecular liquids and the theory of hydrophobic solubilities. *J. Am. Chem. Soc.* 112:5066–5074.

Pratt, L. R., and D. Chandler. 1977. Theory of the hydrophobic effect. *J. Chem. Phys.* 67:3683–3704.

Pratt, L. R., and A. Pohorille. 1992. Theory of hydrophobicity: transient cavities in molecular liquids. *Proc. Natl. Acad. Sci. USA.* 89:2995–2999.

Reynolds, J. A., D. B. Gilbert, and C. Tanford. 1974. Empirical correlation between hydrophobic free energy and aqueous cavity surface area. *Proc. Natl. Acad. Sci. USA.* 71:2925–2927.

Richards, F. M. 1977. Areas, volumes, packing, and protein structure. *Ann. Rev. Biophys. Bioeng.* 6:151–176.

Rosenberg, R. O., R. Mikkilineni, and B. J. Berne. 1982. Hydrophobic effect of chain folding. The *trans* to *gauche* isomerization of *n*-butane in water. *J. Am. Chem. Soc.* 104:7647–7649.

Sitkoff, D., K. A. Sharp, and B. Honig. 1994. Accurate calculation of hydration free energies using macroscopic solvent models. *J. Phys. Chem.* 98:1978–1988.

Smith, D., and A. D. J. Haymet. 1993. Free energy, entropy, and internal energy of hydrophobic interactions: computer simulations. *J. Chem. Phys.* 98:6445–6454.

Smith, P. E., and W. F. van Gunsteren. 1994. Predictions of free energy differences from a single simulation of the initial state. *J. Chem. Phys.* 100:577–585.

Soumpasis, D. M. 1984. Statistical mechanics of the B → Z transition of DNA: contribution of diffuse ionic interactions. *Proc. Natl. Acad. Sci. USA.* 81:5116–5119.

Stillinger, F. H. 1973. Structure in aqueous solutions of nonpolar solutes from the standpoint of scaled-particle theory. *J. Solut. Chem.* 2:141–158.

Tanford, C. 1980. The Hydrophobic Effect. Wiley, New York.

Tobias, D. J., and C. L. Brooks, III. 1990. The thermodynamics of solvaphobic effects: a molecular-dynamics study of *n*-butane in carbon tetra chloride and water. *J. Chem. Phys.* 92:2582–2592.

van Belle, D., and S. J. Wodak. 1993. Molecular dynamics study of methane hydration and methane association in a polarizable water phase. *J. Am. Chem. Soc.* 115:647–652.

Wallqvist, A., and B. J. Berne. 1995. Computer simulation of hydrophobic forces on stacked plates at short range. *J. Phys. Chem.* 99:2893–2899.

Weeks, J. D., D. Chandler, and H. C. Andersen. 1971. Role of repulsive forces in determining the equilibrium structure of simple liquids. *J. Chem. Phys.* 54:5237–5247.

Young, W. S., and C. L. Brooks, III. 1997. A reexamination of the hydrophobic effect: exploring the role of the solvent model in computing the methane–methane potential of mean force. *J. Chem. Phys.* 106:9265–9269.

Zichi, D. A., and P. J. Rossky. 1986. Molecular conformational equilibria in liquids. *J. Chem. Phys.* 84:1712–1723.

Zwanzig, R. W. 1954. High-temperature equation of state by a perturbation method. I. Nonpolar gases. *J. Chem. Phys.* 22:1420–1426.